PERGAMON

International Journal of Heat and Mass Transfer 45 (2002) 279–289

International Journal of HEAT and MASS TRANSFER

www.elsevier.com/locate/ijhmt

Application of a hybrid model of mushy zone to macrosegregation in alloy solidification

Mahmut D. Mat [a,*], Olusegun J. Ilegbusi [b]

[a] *Mechanical Engineering Department, Nigde University, Nigde 51100, Turkey*

[b] *Department of Materials Science and Engineering, Massachusetts Institute of Technology, Cambridge, MA, USA*

Received 28 January 2000; received in revised form 20 April 2001

Abstract

Solidification of an aqueous ammonium chloride (NH_4Cl–H_2O) solution inside a two-dimensional cavity is numerically investigated using a continuum mixture mathematical model. The mushy region where solid and liquid phases co-exist is considered a non-Newtonian fluid below a critical solid fraction, and a porous medium thereafter. This critical solid fraction is chosen as that corresponding to the coherency point, where a solid skeleton begins to form. The numerical results show that the solidification of a hypereutectic NH_4Cl–H_2O solution is mainly characterized by the rejection of solute at the mushy region and double diffusive convection induced by the opposing solutal and thermal buoyancy forces. The mathematical model agrees satisfactorily with the available experimental and numerical data.

1. Introduction

Phase transformation in non-eutectic binary alloys occurs over a temperature range rather than the distinct temperatures in pure systems. Therefore a ''mushy region'' in which solid and liquid phase can coexist forms in such systems. Solute depletion or enrichment may occur in this region due to the difference in the solubility of the solute constituents in the liquid and solid phases. The flow generated by thermal and concentration gradients drives the fluid through and from the mushy region leading to segregation in the system. Considering that most commercial metallic products are in the form of alloys of two or more constituents, the control of flow in the mushy region is critical to improving the quality of the final cast product.

There are mainly three approaches to modeling of solidification of binary alloys. The first approach considers the system as a two-phase mixture of liquid and solid and separate transport equations are solved for both phases. Beckermann and co-workers [1–4] developed sophisticated two-phase models and applied to a range of solidification problems. The second approach considers solidification domain as consisting of three separate regions and solves separate transport equations that are valid in these regions with appropriate boundary conditions between them [5–8]. The third method is the single domain which is based on the solution of a single set of conservation equations and eliminates consideration of separate liquid, solid and mushy regions.

The governing equations in the single domain model or continuum mixture model employed here are very similar to standard single phase flow equations and therefore, are easier to compute than the complete two-phase flow equations. The single domain model also eliminates the need to prescribe complex interfacial boundary conditions and explicit tracking of internal boundaries between the solid, liquid and mushy regions as required in the multidomain method.

Considering two-phase flow equations, Bennon and Incropera [9] developed a continuum equation which accounts for liquid, solid and liquid + solid regions during solidification. The specific nature of the regions are included in the model through appropriate source

* Corresponding author. Tel.: +90-388-225-0115 ext. 507; fax: +90-388-225-0112.

E-mail addresses: mmat@ttnet.net.tr, mdmat@nigde.edu.tr (M.D. Mat), olusegun@mit.edu (O.J. Ilegbusi).

0017-9310/02/$ - see front matter
PII: S0017-9310(01)00150-8

Nomenclature

c_p	specific heat
C	species concentration
D	diffusion coefficient
f	mass fraction
h	enthalpy
H	height of cavity
K	thermal conductivity
K_0	permeability coefficient
k_p	equilibrium partition ratio
P	static pressure
T	temperature
T_e	eutectic temperature
T_m	melting temperature
u	velocity component in x direction
v	velocity component in y direction

Greek symbols

α	thermal diffusivity
β_T	thermal expansion coefficient
β_S	solutal expansion coefficient
μ	dynamic viscosity
ρ	density

terms. The solid fraction is calculated from the phase diagram assuming local thermodynamic equilibrium.

Christienson and Incropera [10] experimentally studied solidification of aqueous NH_4Cl–H_2O solution with a variety of initial solute concentrations. For a hypereutectic solution, it was found that the solute-deficient fluid ejected from the mushy region develops an opposing double diffusive flow. On the other hand, solutal buoyancy forces aid thermal buoyancy forces in hypoeutectic solutions. In a subsequent study, Christenson et al. [11] applied a continuum model and compared with their experimental data. Although this model successfully predicted the basic solidification phenomena, the extent of the solid and mushy regions were underestimated in the study.

Yoo and Viskanta [12] considered anisotropic permeability of the mushy zone, instead of the uniform permeability assumed in many studies. It was shown that permeability significantly affects the solute distribution and the extent of the mushy region. Specifically, a higher permeability in the vertical direction produces higher solute concentration at the top of the cavity. This reduces the liquid temperature and results in significant remelting at the solidification front.

Rady and Nada [13] extended the continuum mixture model to study the free surface effects in solidification of hypereutectic and hypoeutectic ammonium chloride solutions. It was found that free surface effect increases macrosegration in the solidified product, especially for hypoeutectic solutions.

The theoretical models cited above consider the mushy region as a porous medium and apply the Darcy law for the fluid flow. In effect, these models assume that a solid skeleton forms as soon as the solidification is initiated. They are therefore inadequate to represent free floating grain structures, rheocasting, compocasting and DC casting systems. The transport of free equiaxed grains affects the extent of the equiaxed zone and columnar-to-dendritic transition. Sedimentation of floating particles is also largely responsible for structural inhomogeneity in solidified parts. Therefore, treating the full mushy region as a non-moving porous medium physically may not be appropriate at least until the coherency point where dendrites start to impinge and form a solid skeleton during solidification [14,15]. Using rheological methods, Amberg et al. [15] determined the coherency points of several alloys, and found that this value changes between 9% and 30% solid fraction depending on the alloy. It was also shown that near the coherency point, there is a sharp increase in torque measurement indicating formation of a solid structure. The mushy region permeability measurements of Murakami and Okamato [16] and Poirier and Ocansey [17] also support the existence of coherency point in solidifying alloy systems.

In a recent study, Ilegbusi and Mat [18] developed a new hybrid model, which addresses this behavior of the mushy region. The model basically considers the mushy region as a non-Newtonian semi-solid slurry below a critical solid fraction (f_{cr}) and a porous medium thereafter. The new model was shown to perform as satisfactorily as the conventional models. This study did not, however, account for species transfer and hence, did not predict macrosegregation effects and other important phenomena such as double diffusive flow, and remelting occurring during solidification.

The objective of this study is to extend the work of Ilegbusi and Mat [18] to include species transport and apply it to solidification of a binary alloy (NH_4Cl–H_2O) in a two-dimensional cavity. Flow in the system considered is driven mainly by the competing effects of the solutal and thermal buoyancy forces. A continuum model is employed, which is based on a single set of conservation equations that is applicable to the solid, mushy and liquid regions. The continuum approach eliminates the need to prescribe complex interfacial boundary conditions. Solutions are thus subject only to conditions imposed at external boundaries and are capable of predicting important features such as irregular interface morphology and local remelting.

The detailed formulation of the problem is described in the following section (Section 2). Next, the results are presented and discussed in a subsequent section (Section 3). Finally, the major findings of the study are summarized in a concluding section (Section 4).

2. Mathematical formulation

Consideration is given to solidification of an aqueous ammonium alloy (NH_4Cl–H_2O) in a rectangular cavity shown in Fig. 1. This system mirrors the experimental study of Christenson and Incorpera [10] to allow direct comparison of the computed results. Initially, the cavity is filled with a superheated NH_4Cl–H_2O solution with an initial composition of C_{in}. The solidification is induced by suddenly changing the temperature of the left wall to T_{cold} at $t = 0$. The right and left wall temperatures are kept at constant temperatures T_{cold} and T_{hot}, respectively, while the bottom and top walls are assumed to be perfectly insulated.

The continuum model employed to represent the solidification in the cavity is valid in the fully solid, mushy and fully liquid regions. It thus precludes explicit consideration of the phase boundaries.

Within this framework, the equations governing the solidification of a binary alloy in a two-dimensional cavity may be expressed in Cartesian coordinates thus:

Continuity:

$$\frac{\partial}{\partial t}(\rho) + \nabla \cdot (\rho V) = 0. \tag{1}$$

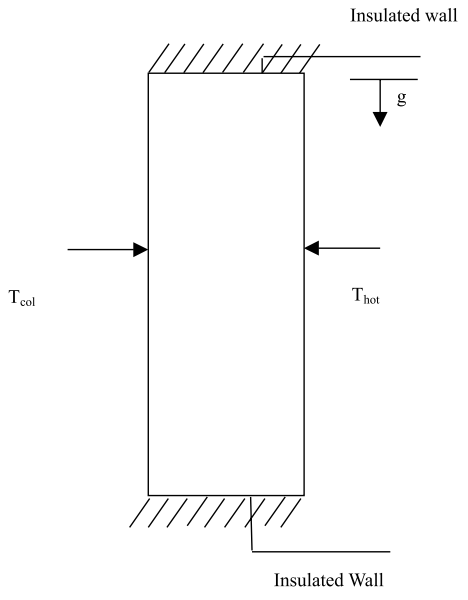

Fig. 1. Schematic sketch of the solidification system considered.

x-Momentum:

$$\frac{\partial}{\partial t}(\rho u) + \nabla \cdot (\rho V u) = -\frac{\partial P}{\partial x} + \nabla \cdot \left(\mu_\ell \frac{\rho}{\rho_\ell} \nabla u\right) + S_X. \tag{2}$$

y-Momentum:

$$\frac{\partial}{\partial t}(\rho v) + \nabla \cdot (\rho V v) = -\frac{\partial P}{\partial y} + \nabla \cdot \left(\mu_\ell \frac{\rho}{\rho_\ell} \nabla v\right) + S_y + S_B. \tag{3}$$

Energy equation:

$$\frac{\partial}{\partial t}(\rho h) + \nabla \cdot (\rho V h) = \nabla \cdot \left(\frac{k}{c_p} \nabla h\right) + S_h. \tag{4}$$

Species conservation:

$$\frac{\partial}{\partial t}(\rho C) + \nabla \cdot (\rho V C) = \nabla \cdot (\rho D \nabla c) + S_c, \tag{5}$$

where ρ is the mixture density, μ_ℓ is the liquid viscosity, c_p is the specific heat of the solid phase, V is the velocity vector whose components are u and v in the present problem, S_x, S_y, S_B, S_h, S_c, are the source terms and will be given in a subsequent section. The variables u, v, h, C are the mixture velocity, enthalpy and concentration, respectively, and defined as

$$u = f_s u_s + f_\ell u_\ell, \tag{6}$$

$$C = f_s C_s + f_\ell C_\ell, \tag{7}$$

$$h = f_s h_s + f_\ell h_\ell, \tag{8}$$

where f_s and f_ℓ represent the mass fraction of solid and liquid phases, respectively, which must sum to unity in the system, thus

$$f_s + f_\ell = 1. \tag{9}$$

2.1. Source terms

Since the continuum equations are valid over the entire solidification regions, the specific nature of the three regions are accounted for through the source terms.

S_β represents the thermal and solutal buoyancy sources expressed as

$$S_\beta = \rho g \lfloor \beta_T (T - T_{ref}) + \beta_S (C_\ell - C_{ref}) \rfloor, \tag{10}$$

where β_T and β_S are the thermal and solutal expansion coefficients, respectively, T_{ref} is the reference temperature and C_{ref} is the reference concentration.

S_h represents the release of latent heat during the phase change. Assuming the specific heat is independent of temperature and composition [12], S_h can be expressed as

$$S_h = -\rho \frac{L}{c_p} \frac{\partial f}{\partial t} + \rho \frac{\Delta c_p}{c_p} \frac{\partial}{\partial t}(f_s T), \tag{11}$$

where L is the latent heat of fusion and

$$\Delta c_p = c_{p\ell} - c_{ps}, \tag{12}$$

where $c_{p\ell}$ and c_{ps} are the specific heats of the liquid and solid phases, respectively.

S_c represents the solute enrichment or depletion at the mushy region due to the difference in the solubility of solute in the liquid and solid phases, given as [9]

$$S_c = \nabla \cdot [\rho f_\ell D_t \nabla (C_\ell - C)] - \nabla \cdot [\rho u (C_\ell - C)]. \tag{13}$$

S_u and S_v represent the momentum source terms, which account for the permeability of the mushy region. Following Ilegbusi and Mat [18], the mushy region is assumed to be a non-Newtonian fluid below a critical solid fraction (coherency point) and a porous region above this threshold. The value of the critical solid fraction is chosen based on the experimental results of Amberg et al. [15] on the coherency point at which a solid skeleton begins to form in the solidifying system. This value was found to vary between 9% and 30% solid fraction depending on the alloy system. Since this value is not available for the NH_4Cl–H_2O system considered here, the coherency point has been chosen to be at the upper limit of Arnberg's data, i.e., $f_s = 0.3$. This may be considered realistic, being closer to the equivalent packing density of 0.54 for perfectly spherical solid particles. The mushy region is treated as a power-law fluid below $f_s = 0.3$ and the viscosity is calculated from the following relation [19]:

$$\mu = m \left| \frac{1}{2} (\Delta : \Delta)^{1/2} \right|^{n-1} \tag{14}$$

in which $\Delta : \Delta$ represents the dyadic product of deformation rate tensor, expressed as

$$\frac{1}{2}\Delta : \Delta = 2\left(\left(\frac{\partial u}{\partial x} \right)^2 + \left(\frac{\partial v}{\partial y} \right)^2 \right) + \left(\frac{\partial u}{\partial x} + \frac{\partial v}{\partial y} \right)^2, \tag{15}$$

where m and n are empirical constants given by [18]

$$m = \exp(9.783 f_s + 1.435), \tag{16}$$

$$n = 0.105 + 0.41 f_s. \tag{17}$$

Above the coherency point, the mushy region is assumed to obey the Darcy law for a porous medium. Thus the source terms S_x and S_y in the momentum equations (Eqs. (2) and (3)) can be expressed as

$$S_x = KH^2 u/\rho, \tag{18}$$

$$S_y = KH^2 v/\rho, \tag{19}$$

where K is the permeability of the mushy region calculated using the Carmen–Kozeny relation [20]

$$K = K_0 \frac{f_s^2}{(1 - f_s)^3}, \tag{20}$$

where K_0 is a coefficient that depends on the morphology and alloy composition.

2.2. Thermodynamic relations

The local mass fraction, liquid and solid concentration are calculated assuming local thermodynamic equilibrium in the system. Neglecting curvature on the solidus and liquidus curves, the liquid and solid mass fraction can be expressed as

$$f_\ell = 1 - \frac{1}{1 - k_p} \frac{T - T_{liq}}{T - T_m}, \tag{21}$$

$$f_s = 1 - f_\ell, \tag{22}$$

where T_m is the melting temperature of pure NH_4Cl, and T_{liq} is the liquidus temperature calculated from

$$T_{liq} = T_m + (T_e - T_m) \frac{C}{C_e}. \tag{23}$$

Assuming local thermodynamic equilibrium, solid and liquid temperatures at the solid–liquid interface must satisfy the relation

$$T_s = T_\ell = T. \tag{24}$$

Phase compositions are linked to the liquid faction and mixture concentration, thus

$$C_s = \frac{k_p C}{1 + (1 - f_\ell)(k_p - 1)}, \tag{25}$$

$$C_\ell = \frac{C}{1 + (1 - f_\ell)(k_p - 1)}, \tag{26}$$

where k_p is the partition ratio.

2.3. Initial and boundary conditions

The superheated fluid is initially motionless and has a uniform temperature T_{in} and concentration C_{in}. The initial conditions can thus be expressed mathematically as

$$t = 0: \quad u = v = 0, \quad C = C_{in}, \quad T = T_{in}. \tag{27}$$

Solidification is induced by keeping the left and right walls at constant temperatures, T_{hot} and $T_{cold} (< T_m)$, respectively, while adiabatic conditions are maintained on the other walls. The walls are assumed to be impermeable and the no-slip condition is imposed. These boundary conditions can be expressed mathematically as

$$x = 0: \quad u = v = 0, \quad T = T_{cold}, \quad \frac{\partial C}{\partial x} = 0, \tag{28}$$

$$x = L: \quad u = v = 0, \quad T = T_{hot}, \quad \frac{\partial C}{\partial x} = 0, \tag{29}$$

$$y = 0: \quad u = v = 0, \quad \frac{\partial T}{\partial y} = 0, \quad \frac{\partial C}{\partial y} = 0, \tag{30}$$

Table 1
Thermophysical properties of NH_4Cl–H_2O and data used in the computations

		Solid	Liquid
Density	(kg/m^3)	1078	1078
Specific heat	(J/kg K)	1870	3249
Thermal conductivity	(W/m K)	0.393	0.468
Diffusion coefficient	(m^2/s)	–	4.8E − 5
Viscosity	(kg/m s)	–	1.3E − 3
Latent heat of fusion	(J/kg)	–	3.138E − 4
Thermal expansion coefficient	(K^{-1})	–	3.032E − 4
Solutal expansion coefficient		–	0.257
Eutectic temperature	(K)	257.75	
Eutectic composition		0.803	
Equilibrium partition ratio		0.3	
Width of cavity	(m)	0.036	
Height of cavity	(m)	0.144	
T_{in}	(K)	243	
T_{hot}	(K)	243	
T_{cold}	(K)	213	
C_{in}		0.69	

$$y = L: \quad u = v = 0, \quad \frac{\partial T}{\partial y} = 0, \quad \frac{\partial C}{\partial y} = 0. \tag{31}$$

The thermophysical properties of NH_4Cl–H_2O solution and values of the data used in the calculations are given in Table 1.

2.4. Computational details

The governing equations are solved numerically with a fully implicit, finite-domain scheme embodied in the PHOENICS computer code [21]. The solution procedure involves integration of the differential equations over finite control volumes into which the system has been discretized, transforming them into a general algebraic form

$$a_p \Psi_p = \sum a_k \Psi_k + a_0 \Psi_p^0 + S_\Psi, \tag{32}$$

where Ψ represents the generic variables solved (u, v, h, c), Ψ_p is the unknown nodal value, Ψ_p^0 represents Ψ_p at an earlier time, subscript k designates the neighboring nodes linking node p, a represents the combined advection and diffusion coefficients, and S_Ψ is a component of the linearized source term.

The code employs a staggered grid arrangement in which velocities are located at the faces of the control volume. The velocity–pressure coupling is handled by a SIMPLE type algorithm [22].

Discretizing the convection/diffusion source terms in the species conservation equation requires special attention to ensure the total amount of species is conserved throughout the solidification process. This is achieved using methodology proposed by Bennon and Incropera [9] in which the convective and diffusive link coefficients are employed in the finite difference equations. Another important issue is the method of calculating the temperature since it explicitly depends on the solid fraction and concentration. In this study a solid fraction-temperature updating scheme [20] is used.

A 40×40 non-uniform spatial grid system is employed in the computations following a systematic grid independence test. A typical result is presented in Fig. 2, showing the temperature profile calculated using 10×10, 30×30, 40×40 and 50×50 grid systems at $y = h/2$ after 5 min of solidification. It is seen that changes in temperature profile is not significant beyond the 40×40 grid system. A similar test was performed to choose the temporal step of 0.5 s. A constant viscosity is assumed in the first sweep of the first timestep to obtain a preliminary deformation rate and viscosity. The calculations are then repeated until a fully converged result is obtained. The results are considered fully converged when changes in the temperature, velocities and con-

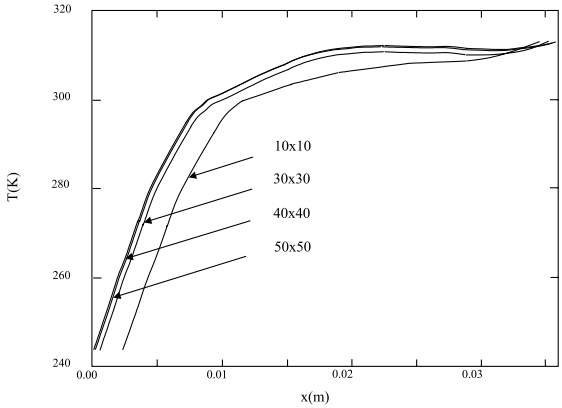

Fig. 2. Grid independence test (T at $y = H/2$, $t = 5$ min).

centration fall below 10^{-6}. The computations are performed on a Pentium II PC and 1 min of real time simulation takes about 30 min of CPU time.

3. Results

The evolution of the solidification of Aqueous NH_4Cl–H_2O alloy is presented in Fig. 3 at four representative time spans of $t = 1, 5, 8$ and 15 min, respectively. The results after 15 min are not included because a steady-state condition has been reached in the numerical sense.

Fig. 3(a) shows the flow field, temperature and solute distribution, one minute after the solidification is initiated. The flow field is illustrated in terms of the velocity vectors and streamlines. The isotherms and isoconcentration curves are plotted with 10 equal increments

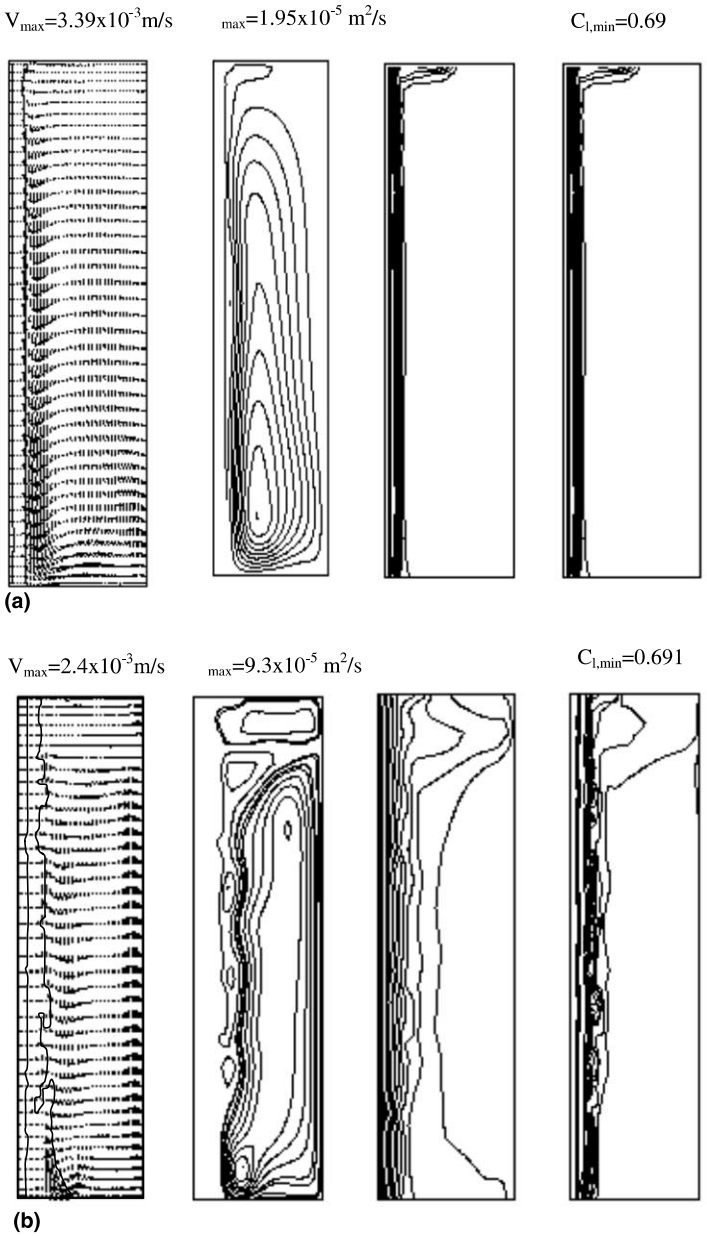

Fig. 3. Predicted velocity field, streamlines, isotherms and isoconcentrations at: (a) $t = 1$ min; (b) $t = 5$ min; (c) $t = 8$ min; (d) $t = 15$ min.

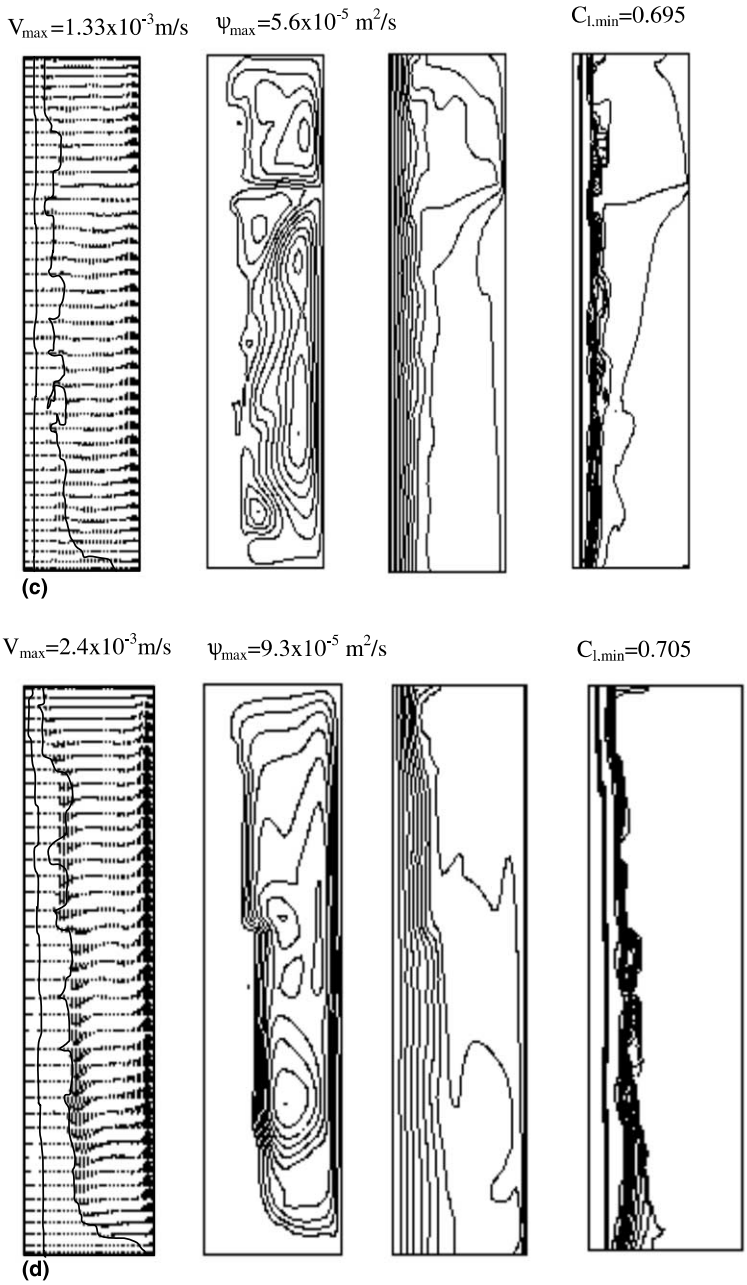

Fig. 3 *(continued)*

between the maximum and minimum values of the temperatures and concentrations in the cavity. The mushy zone is marked on the velocity vectors between solid mass fraction values of 0.01 and 0.99. It is seen that two circulation patterns of opposite directions are formed in the cavity. A thermally induced circulation due to the temperature gradient between the hot and cold walls rotates counter clockwise and fills most of the cavity. Another circulation develops due to the concentration gradient in the mushy region and rotates in the clockwise direction.

The isoconcentration lines show that excess water that is rejected from the mushy region due to the difference in solubility of water in the solid and liquid phases rises to the top of the cavity and forms a water-rich layer. The temperature of this layer also decreases

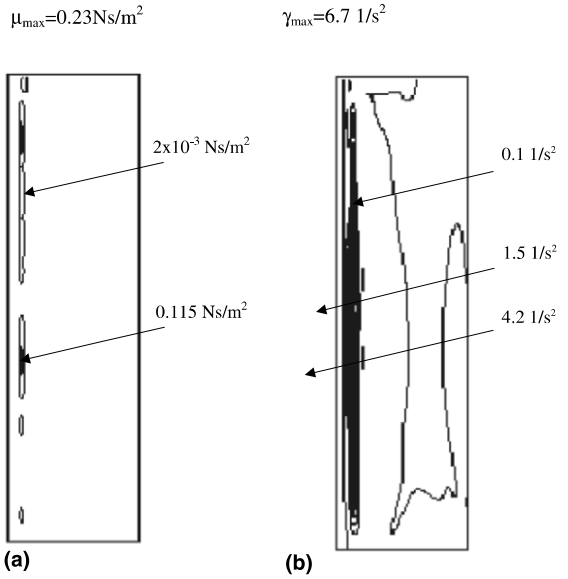

Fig. 4. Predicted viscosity (a) and deformation rate (b) distribution in the cavity at $t = 1$ min.

as a result of the lower temperature of this rejected water. The solute concentration in the liquid phase remains uniform at the initial value.

The solidification pattern at $t = 5$ s is shown in Fig. 3(b). The flow is again similar to that for $t = 1$ s in Fig. 3(a). The water rejected from the mushy region continually accumulates at the top of the cavity and therefore a water-rich layer grows downwards. A small thermally induced circulation develops in this layer and a solutal buoyancy induced flow is apparent between the upper and lower thermally induced circulations. The effect of thermal buoyancy is quite evident in this figure. Specifically, the flow generated by thermal buoyancy distorts the isotherms close to the bottom wall. The isotherms in the solid region are straight lines and consistent with pure conduction. It is interesting that concentration gradients, unlike thermal gradients, occur only at the top of the cavity, indicating that solutal buoyancy is most effective in the mushy region. The size of the mushy region also increases, indicating a progression of solidification in the system. The high water concentration at the top of the cavity results in a decrease in the liquidus temperature and local remelting. Thus the solidification front does not advance significantly in this region. The liquidus front exhibits an irregular behavior and a pocket-like structure forms in the mushy region, representing the preferred flow passage for interdendritic fluid. This type of structure was also observed in the experimental works of Szekely and Jassal [23] and Yoo and Viskanta [12].

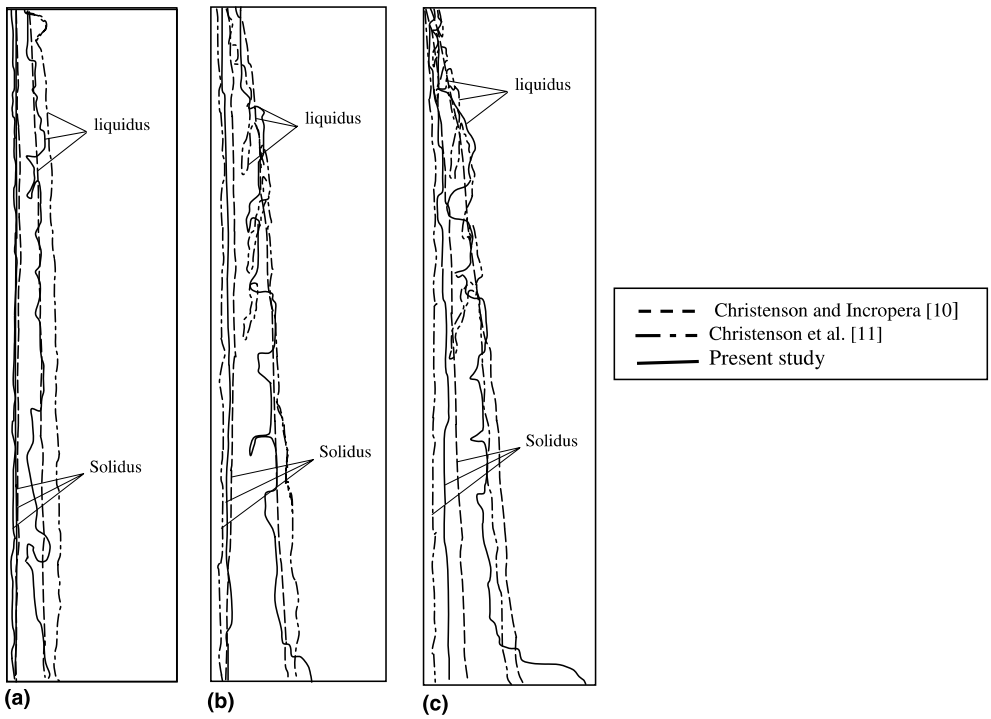

Fig. 5. Comparison of predicted structure of mushy region with experimental results of Christenson and Incropera [10] and numerical results of Christenson et al. [11]: (a) $t = 3$ min; (b) $t = 11$ min; (c) $t = 15$ min.

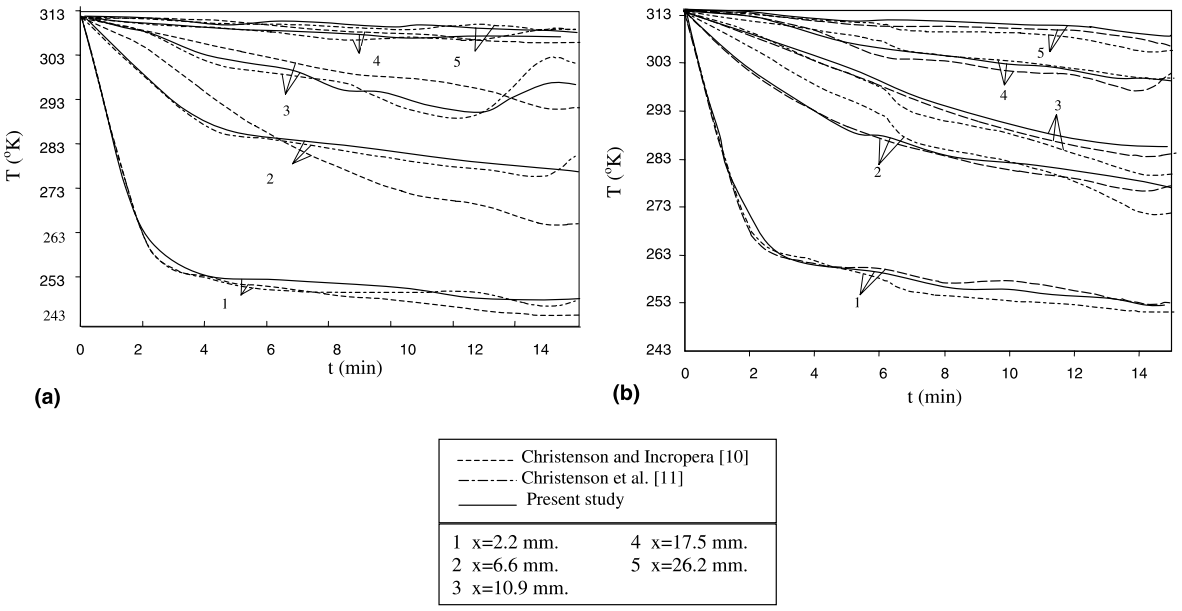

Fig. 6. Comparison of predicted temperature histories along the x axis with experimental and numerical data: (a) $y = 45$ mm; (b) $y = 90$ mm.

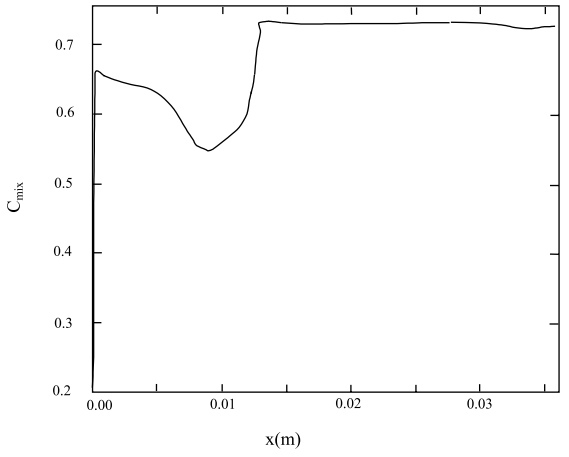

Fig. 7. Final macrosegregation along the cavity at $y = H/2$.

Solute enriched top layer continually grows at a later stage of solidification ($t = 8$ min). The mushy region is wider especially at the lower section of the cavity. This may be attributed to thermal convection which drives the colder fluid in a counter-clockwise direction at the bottom of the cavity. Another contributing factor is the settling of free-floating grains in the mushy region. This important phenomenon occurring during the alloy solidification is adequately captured by the present model.

At $t = 15$ min, the circulation at the top of the cavity has grown into a thermally induced circulation, forming a single counter-clockwise circulation. The isotherms and isoconcentration lines show that this single circulation homogenizes the temperature and concentration fields in the cavity. The numerical results do not change significantly beyond $t = 15$ min, indicating that steady state has been attained. Thus, subsequent results are not presented here for brevity.

Fig. 4 shows the distribution of deformation rate in the cavity at $t = 1$ min. The field is divided into 10 equal intervals. It is seen that the deformation rate is highest close to the mushy region and smallest at the top and lower sections of the cavity. The higher deformation in front of the liquidus line indicates that the dendrite arms in this vicinity will be subjected to large shear that may result in their breakup. The low deformation regions represent possible regions of accumulation of broken dendrite arms. The corresponding viscosity isopleths at $t = 5$ min are shown in Fig. 4(b). The viscosity of the mushy zone is low in the regions subjected to high deformation rates. This result is consistent with the assumed shear thinning behavior of the mushy zone.

The predicted extent of the mushy region is compared with the experimental results of Christenson and Incropera [10] and numerical results of Christenson et al. [11] in Fig. 5. The mushy region is demarcated between solid fraction values of 0.01 (liquidus line) and 0.99 (solidus line). Both predictions are in good agreement with the experimental results at $t = 3$ min. However, Christenson et al. [11] slightly overestimate the liquidus front at this stage. The present model predicts an irregular interface while the other two results [10,11] ex-

hibit quite smooth interfaces. The experimental results [10] may be attributed to the smoothing of the data.

Fig. 5(b) shows that the three results agree very well at $t = 11$ min but the solidus front is slightly underestimated in the numerical results. Both numerical results capture the irregularities (i.e. flow channels) on the liquidus line, but the predicted locations of channels differ. The difference between the two numerical results is most evident at $t = 15$ min. It is seen that the present study captures the solidus line better than Christenson et al. [11]. The liquidus front is overpredicted by the present model at the bottom of the cavity. This is consistent with the experimental result of Yoo and Viskanta [12] and was associated with the settling of free grains and broken dendrite arms in the mushy region. Such trend was not detected in the experiment of Christenson and Incropera [10], perhaps due to an error in their experimental technique. Furthermore, the difference in the numerical results is a result of the allowance in the present model for motion of broken dendrites and free grains in the mushy region.

The predicted temperature histories are compared with the experimental data of Christenson and Incropera [10] and numerical results of Christenson et al. [11] in Fig. 6. The temperature is measured along the x-axis at two heights of $y = 45$ mm and $y = 90$ mm where the most important phenomena occur during the solidification. Both numerical results are generally in agreement with the experimental data.

Fig. 7 shows the predicted mixture concentration with distance from the cooled solid surface at a late stage of solidification ($t = 15$ min). This result clearly shows the existence of a diffusion boundary layer on the cooled wall resulting from the allowance for solute diffusion in the liquid phase in our model. The mechanism of formation this boundary layer was first reported by Schneider and Beckermann [24] and discussed in detail by Thevik and Mo [25] and recently by Kuznetsov [26]. It was attributed to solute rejection from interdendritic fluid due to the positive temperature gradient adjacent to a cooled wall. Since the wall is impermeable, this depleted solute cannot be compensated and a thin diffusion layer forms there as shown in Fig. 7.

4. Conclusion

The solidification of an aqueous ammonium chloride solution in a two-dimensional cavity has been numerically studied. A continuum mixture mathematical model is employed, which is valid in the solid, liquid and mushy regions. The mushy region is considered a non-Newtonian fluid below a critical solid fraction and a porous medium thereafter. This critical solid fraction is chosen at the coherency point where a solid skeleton begins to form in the mushy region.

The solidification of a hypereutectic binary alloy is characterized by several factors. These factors include solute rejection in the mushy region due to the different solubities of water in the solid and liquid phases, an opposing buoyancy flow that is generated by concentration gradient and thermal gradient in the cavity, remelting, formation, growth and break-up of solute-rich layer at the top of the cavity and irregular liquidus front.

The predicted deformation rate is high near the liquidus front in the mushy region and this may cause a break-up of dendrite arms. The viscosity is relatively high in the quiescent regions. The present model predicts a smoother liquidus interface at the late stage of solidification than a numerical study that is based on a fully porous medium model. In addition, a larger mushy region is predicted at the bottom of the cavity by the present model compared to the conventional model. This is due to the allowance for motion of free floating particles and broken dendrites in the former situation.

Although the rheology of the mushy region has been adapted from studies on alloy systems for which experimental data exist, the present model has demonstrated the potential to capture the main features of alloy solidification in general. The results provide insight into the physics of such problems over existing models that are based on fully porous media. However, detailed experimental studies are still required to establish the model constants. It is also desirable to apply the model to other alloy systems to establish its universality.

Acknowledgements

This work is partly supported by the Scientific and Technical Research Council of Turkey (TUBITAK) under contract number MISAG-124.

References

[1] J. Ni, C. Beckermann, A volume-averaged two-phase model for transport phenomena during solidification, Metall. Mater. Trans. B 22 (1991) 349–361.
[2] J. Ni, C. Beckermann, Modeling of globulitic alloy solidification with convection, J. Mater. Process. Mater. Sci. 2 (1993) 217–231.
[3] C.Y. Wang, C. Beckermann, Equiaxed dendritic solidification with convection: Part 1. Multi-scale/-phase modelling, Metall. Mater. Trans. A 27 (1996) 2754–2764.
[4] C. Beckermann, H.J. Diepers, I. Steinbach, A. Karma, X. Tong, Modeling melt convection in phase-field simulations of solidification, J. Comput. Phys. 154 (1999) 468–496.
[5] V.R. Voller, Development and application of a heat balance integral method for analysis of metallurgical solidification, Appl. Math. Model. 13 (1989) 3–11.
[6] M.G. Worster, Instabilities of the liquid and mushy region during directional solidification of alloys, J. Fluid Mech. 237 (1992) 649–669.

[7] P.W. Emms, A.C. Fowler, Compositional convection in the solidification of binary alloys, J. Fluid Mech. 262 (1994) 111–139.
[8] V.R. Voller, A similarity solution for the solidification of a multicomponent alloy, Int. J. Heat Mass Transfer 40 (1997) 2869–2877.
[9] W.D. Bennon, F.P. Incropera, A continuum model for momentum heat and species transport in binary solid–liquid phase change systems – II. Application to solidification in a rectangular cavity, Int. J. Heat Mass Transfer 30 (1987) 2171–2187.
[10] M.S. Christenson, F.P. Incropera, Solidification of an aqueous ammonium chloride solution in a rectangular cavity – I. Experimental study, Int. J. Heat Mass Transfer 32 (1989) 47–68.
[11] M.S. Christenson, W.D. Bennon, F.P. Incropera, Solidification of an aqueous ammonium chloride solution in a rectangular cavity – I. Comparison of predicted and measured results, Int. J. Heat Mass Transfer 32 (1989) 69–79.
[12] H. Yoo, R. Viskanta, Effect of anisotropic permeability on the transport process during solidification of a binary mixture, Int. J. Heat Mass Transfer 35 (1992) 2335–2346.
[13] M.A. Rady, S.A. Nada, Solidification of hypereutectic and hypoeutectic binary alloys with buoyancy and surface tension driven natural convection, Res. J. Heat Mass Transfer 34 (1998) 337–347.
[14] A.S. Sabau, Q. Han, S. Viswanathan, Projection methods for interdendritic flow, in: N. El-Kaddah, D.G.C. Robertson, S.T. Johansen, V.R. Voller (Eds.), Fluid Flow Phenomena in Metal Processing, 1999, pp. 403–411.
[15] L. Arnberg, G. Chai, L. Backerud, Determination of dendritic coherency in solidifying melts by rheology measurements, Mater. Sci. Eng. A 173 (1993) 101–103.
[16] K. Murakami, T. Okamoto, Fluid flow in the mushy zone composed of granular grains, Acta Metall. 32 (1984) 1741–1744.
[17] D.R. Poirier, P. Ocansey, Permeability for flow of liquid through equiaxial mushy zones, Mater. Sci. Eng. A 171 (1993) 231–240.
[18] O.J. Ilegbusi, M. Mat, A hybrid model of mushy region in phase-change problems, J. Mater. Process. Manuf. Sci. 5 (1997) 209–223.
[19] O.J. Ilegbusi, Application of a time dependent constitutive model to rheocast systems, J. Mater. Eng. Performance 5 (1996) 117–123.
[20] C. Prakash, V. Voller, On the numerical solution of continuum mixture model equations describing binary solid–liquid phase change, Numer. Heat Transfer B 15 (1989) 171–189.
[21] H. Rosten, D.B. Spalding, PHOENICS Manual, CHAM, TR/100, London, UK, 1986.
[22] S.V. Patankar, Numerical Heat Transfer and Fluid Flow, McGraw-Hill, New York, 1980.
[23] I. Szekely, A.S. Jassal, An experimental and analytical study of the solidification of a binary dendritic system, Metall. Trans. B 9 (1978) 389–398.
[24] M.C. Schneider, C. Beckermann, A numerical study of the combined effects of microsegregation, mushy zone permeability and flow, caused by volume contraction and thermosolutal convection, on macrosegregation and eutectic formation in binary alloy solidification, Int. J. Heat Mass Transfer 38 (1995) 3455–3473.
[25] H.J. Thevik, A. Mo, The effect of macroscopic solute diffusion in the liquid upon surface macrosegregation, Metall. Trans. B 28 (1997) 665–669.
[26] A.V. Kuznetsov, Numerical investigation of the macrosegregation during thin strip casting of carbon steel, Numer. Heat Transfer B 33 (1998) 515–532.